Photoinduced Mass-Migration Behavior of Two Amphiphilic Side-Chain Azo Diblock Copolymers with Different Length Flexible Spacers

Dongrui Wang, Gang Ye, Yu Zhu, and Xiaogong Wang*

Department of Chemical Engineering, Laboratory for Advanced Materials, Tsinghua University, Beijing 100084, P. R. China

Received November 19, 2008; Revised Manuscript Received February 4, 2009

ABSTRACT: This article reports the synthesis and photoinduced mass-migration behavior of two amphiphilic side-chain azo diblock copolymers (PEG-*b*-P2CN, PEG-*b*-P6CN), which contain ethylene and hexamethylene as flexible spacers between main chains and pendent azobenzene functional groups. The copolymers were synthesized by atom transfer radical polymerization (ATRP) to obtain precursor block copolymers from a PEG-based macromolecular initiator and postpolymerization azo-coupling reaction of the precursors to introduce the azo chromophores. Spectroscopic analyses, GPC, and thermal analyses indicated that the diblock copolymers possessed well-defined structures and narrow molecular weight distributions. The photoinduced mass-migration behavior was studied through two different approaches, that is, investigating photoinduced deformation of colloidal spheres of the copolymers and surface relief grating (SRG) formation on the polymer thin films. The colloidal spheres used for the light irradiation experiments were prepared by solvent-induced phase separation and set on the substrates (such as TEM copper grids) as solid particles. Upon irradiation with a linearly polarized Ar^+ laser beam (488 nm, 150 mW/cm^2), the colloidal spheres of both copolymers were gradually elongated in the polarization direction of the laser beam, which evidenced the photoinduced mass migration on the micrometer scale. In the process, the PEG-*b*-P2CN colloids showed a significantly larger deformation rate and degree compared with the PEG-*b*-P6CN colloids. The mass-migration ability was also tested by inscribing surface relief gratings on PEG-*b*-P2CN and PEG-*b*-P6CN films with interfering Ar^+ laser beams. The PEG-*b*-P2CN showed a significantly faster rate of grating formation and larger modulation depth in comparison with the PEG-*b*-P6CN. The observations suggest that the flexible spacer could play an important role in transferring the light-driving force from the azo chromophores to the polymer backbones, where the shorter spacers showed a more significant effect to cause the mass migration.

Introduction

Azobenzene-containing polymers (azo polymers for short) have been intensively investigated in the past decades for their unique properties and potential applications in data storage, sensors, and other optical devices.[1−5] Owning to the trans−cis photoisomerization of azobenzenes, azo polymers can show a variety of photoresponsive variations, such as phase transition,[6] chromophore orientation,[7] surface relief grating (SRG) formation,[8,9] and photomechanical bending of thin films.[10−13] A variety of azo polymers with different molecular architecture, such as amorphous polymer,[14,15] liquid crystal (LC) polymers,[10−13,16] dendritic and hyperbranched polymers,[17−20] and block copolymers,[21−24] have been synthesized. The structure−property relationship of the azo polymers has been widely explored to understand the correlation between polymer structure and the photoresponsive behavior. The influence of structural factors on many of the properties has been well documented in the literature.[3−5] The knowledge base has been used for material property improvement and mechanism elucidation.[25,26]

Photoinduced mass migration as a unique property of azo polymers has attracted considerable attention in recent years.[3,4,8,9] As the earliest well-documented instance of this photoeffect, it has been reported that SRGs can be induced on azo polymer films upon irradiation with interfering Ar^+ laser beams.[8,9] The SRGs form at a temperature below the glass-transition temperature (T_g) of the polymers and are erasable by thermal treatment or irradiation with a uniform circularly polarized laser beam. Much evidence shows that the reversible surface modulation is caused by photoinduced mass migration at the polymer film surfaces.[3,4] Although different models and theories have been proposed to elucidate the driving force, the exact mechanism that causes the mass migration is still a debatable issue.[27−31] Recently, it has been observed by us and other groups that light irradiation can cause significant shape deformation of colloidal spheres of azo polymers.[32,33] When the colloidal spheres were irradiated with polarized Ar^+ laser single beam or interfering beams, the colloids could be significantly stretched along the polarization direction of the laser beam. Before saturation, the deformation degree almost linearly increased with the increase in the irradiation time. The colloid deformation can also be attributed to the photoinduced migration of azo polymer chains on the micrometer scale. In the current stage, a study of the structure−property relationship is still required to understand the common nature and mechanism of the photoinduced phenomena.

Flexible spacers between polymer main-chain and pendent side-chain functional groups play an important role in determining properties of functional polymers.[34−43] The spacer length in side-chain LC polymers can predominantly determine the mesophase types and properties.[34−37] The influence of the spacer length on photoinduced polarization has been studied for different types of azo polymers.[38−43] It has been observed that upon irradiation with linearly polarized UV light, the alignment of azo chromophores is more difficult to be induced for azo polymers with shorter spacers.[38,39] As the alkylene spacer length increases, the azobenzene groups show an enhanced tendency to orient homeotropically upon the irradiation with nonpolarized light.[40] However, it has been reported that the maximum and remnant levels of photoinduced birefringence decrease with the increase in the spacer length for a series of side-chain azo

* Corresponding author. E-mail: wxg-dce@mail.tsinghua.edu.cn.

10.1021/ma8026063 CCC: $40.75
Published on Web 03/04/2009

polymethacrylates with different spacers.[41] These results have been attributed to the cooperative orientation of the side chain and backbone, where the spacer length is an important structural factor that influences the properties.[42,43] Therefore, it is of considerable interest to understand whether the flexible spacers can show influences on the photoinduced mass migration appearing as colloid deformation and SRG formation. However, to our knowledge, a systematic study concerning the spacer length influence on this type of photoresponsive properties is still lacking in the literature.

In this work, we studied the photoinduced mass-migration behavior of two azobenzene-containing diblock copolymers (PEG-*b*-P2CN, PEG-*b*-P6CN) that possessed ethylene and hexamethylene as flexible spacers between main chains and pendent azo chromophores. The synthesis of PEG-*b*-P2CN, which was prepared through atom transfer radical polymerization (ATRP) and postpolymerization azo-coupling reaction, was reported in our previous article.[44] In the current study, a new azobenzene-containing block copolymer (PEG-*b*-P6CN) with hexamethylene spacer was synthesized through a similar procedure. Upon irradiation of a linearly polarized Ar^+ laser beam (488 nm, 150 mW/cm^2), the colloidal spheres of PEG-*b*-P2CN showed an obviously faster deformation rate and larger deformation degree compared with those of the PEG-*b*-P6CN colloids. When being irradiated with interfering Ar^+ laser beams, PEG-*b*-P2CN also showed a significantly faster rate for SRG formation and larger modulation depth than PEG-*b*-P6CN. The experimental details, results, and discussion will be presented in the following parts.

Experimental Section

Materials. Poly(ethylene glycol) monomethyl ether with a number-average molecular weight of about 5000 (Fluka) was purified by azeotropic distillation with toluene before use. Copper(I) bromide (98%, Acros) was first washed with excess acetic acid, followed by washing with ethanol and ether, and it was then dried. Anisole was distilled over calcium hydride prior to use. Tetrahydrofuran (THF) was purified by distillation with sodium and benzophenone. Deionized water (resistivity >18 MΩ·cm) was obtained from a Milli-Q water purification system. All other reagents and solvents were purchased commercially and used without further purification.

Block Copolymer Synthesis and Characterization. Poly(ethylene glycol)-*b*-poly(2-(*N*-ethyl-*N*-(4-(4′-cyanophenylazo)phenyl)amino)ethyl methacrylate) (PEG-*b*-P2CN) and poly(ethylene glycol)-*b*-poly(6-(*N*-methyl-*N*-(4-(4′-cyanophenylazo)phenyl)amino)-hexyl methacrylate) (PEG-*b*-P6CN) were obtained first through ATRP initiated by a macroinitiator (PEGBr) to yield poly(ethylene glycol)-*b*-poly(2-(*N*-ethyl-*N*-phenylamino)ethyl methacrylate) (PEG-*b*-PEMA) and poly(ethylene glycol)-*b*-poly(6-(*N*-methyl-*N*-phenylamino)hexyl methacrylate) (PEG-*b*-PHMA). Then, the precursor copolymers were reacted with diazonium salt of 4-aminobenzonitrile to produce the target block copolymers. The macroinitiator PEGBr was obtained by a reaction between poly(ethylene glycol) monomethyl ether and 2-bromo-2-methylpropionyl bromide. The preparation of PEGBr and 2-(*N*-ethyl-*N*-phenylamino)ethyl methacrylate (EMA) was given in our previous report.[45a] The synthesis and characterization of PEG-*b*-P2CN have been reported in detail elsewhere.[44] The preparation and characterization of 6-(*N*-methyl-*N*-phenylamino)hexyl methacrylate (HMA) are given in the Supporting Information. The synthesis and characterization of PEG-*b*-P6CN are given as follows.

PEG-*b*-PHMA. The block precursor copolymer was prepared through ATRP by using PEGBr as the macroinitiator, which had the repeat unit number of 122 estimated from the ^{1}H NMR spectrum. PEGBr (0.275 g, 0.05 mmol) and CuBr (28.8 mg, 0.2 mmol) were added to a 25 mL Schlenk flask. Then, it was degassed and back-filled with argon three times. After that, anisole (10 mL), HMA (2.75 g, 10 mmol), and 1,1,4,7,10,10-hexamethyltriethylenetetramine (HMTETA) (54.4 μL, 0.2 mmol) were added in turn via gastight syringes. After it was degassed by three freeze−pump−thaw cycles, the flask was immersed in an oil bath to carry out the reaction at 80 °C for 20 h. The reaction was stopped by dilution with THF, and the mixture was passed through an alumina column to remove the catalyst. The product was purified twice by precipitation in hexane and then dried in a vacuum oven for 24 h. Yield: 1.78 g polymer, 59%. M_n(GPC) = 32 300, M_w/M_n = 1.19, and M_n(NMR) = 49 200. ^{1}H NMR ($CDCl_3$ δ): 0.70−1.10 (m, 3H), 1.31 (m, 4H), 1.56 (m, 4H), 1.65−2.05 (m, 2H), 2.89 (s, 3H), 3.26 (t, 2H), 3.64 (m, PEG H), 3.87 (t, 2H), 6.72 (m, 3H), 7.26 (t, 2H). The repeat unit number of PHMA block was 159 estimated from the ^{1}H NMR spectrum.

PEG-*b*-P6CN. The azo diblock copolymer was prepared through an azo-coupling reaction between PEG-*b*-PHMA and diazonium salt of 4-aminobenzonitrile. An aqueous solution of sodium nitrite (0.06 g, 0.87 mmol) was added dropwise to a solution of 4-aminobenzonitrile (0.089 g, 0.75 mmol) in a homogeneous mixture of sulfuric acid (0.15 mL) and glacial acetic acid (2.25 mL). The mixture was stirred at 0 °C for 5 min. Then, the diazonium salt solution was added dropwise to a solution of PEG-*b*-PHMA (0.155 g, 0.5 mmol in terms of the aniline group) in DMF (30 mL) at 0 °C. After the reaction was carried out at 0 °C for 12 h, the solution was poured in an excess amount of water. The precipitate was collected by filtration and washed with water repeatedly. After it was dried, the product was dissolved in THF and then precipitated in hexane. The precipitate was collected and then dried in a vacuum oven for 24 h. Yield: 0.12 g polymer, 55%. M_n(GPC) = 34 000, M_w/M_n = 1.23, and M_n(NMR) = 69 700. ^{1}H NMR ($CDCl_3$ δ): 0.75−1.10 (m, 3H), 1.26 (m, 4H), 1.53 (m, 4H), 1.70−2.00 (m, 2H), 2.92 (s, 3H), 3.27 (t, 2H), 3.64 (m, PEG H), 3.87 (t, 2H), 6.60 (d, 2H), 7.62 (d, 2H), 7.76 (m, 4H).

Sample Preparation. The diblock copolymers, PEG-*b*-P2CN and PEG-*b*-P6CN, were first dissolved in anhydrous THF (a good solvent for both blocks) to obtain solutions with concentrations of 0.2 g/L. Then, deionized water (1 mL) was slowly added to the polymer solutions (1 mL) via a syringe pump under different water addition rates. During the process, the containers were kept at room temperature with gentle stirring. The critical water contents (CWCs) were obtained by measuring the light scattering intensity at an angle of 90°. After the water addition was completed, another 9 mL of water was added to the dispersions to quench the formed colloidal structures. We obtained stable dispersions by removing THF at room temperature under a dust-free air ambience condition for 48 h. We prepared the colloidal samples used for laser irradiation by casting a droplet of the diluted colloidal dispersions on a TEM copper grid and drying under the ambient condition. We obtained thin films used for SRG inscription by dissolving PEG-*b*-P2CN and PEG-*b*-P6CN in DMF (10 wt %). The solutions were filtered with 0.45 μm syringe filters and then spin-coated onto clean glass substrates at the rate of 2000 rpm. The films were allowed to dry in a vacuum oven at 40 °C for 24 h.

Laser Light Irradiation Experiments. A linearly polarized Ar^+ laser beam (488 nm, 150 mW/cm^2), which was expanded and collimated, was used as the light source. The colloid spheres on the copper grids were irradiated with the Ar^+ laser beam incident in the perpendicular direction for different time periods. The shape deformation was characterized by TEM observation. The SRGs were inscribed by an experimental setup similar to that reported before.[8,9] A *p*-polarized Ar^+ laser beam (488 nm, 150 mW/cm^2), obtained after expansion and collimation, was used as the light source. Half of the collimated beam was incident onto the films directly and the other half of the beam was reflected onto the films from a mirror. We monitored the grating inscription by measuring the growth of the first-order diffracted efficiency over time, which was obtained by an unpolarized low-power He−Ne laser beam (633 nm) in transmission mode. We recorded the surface profiles of the gratings by using AFM in the tapping mode.

Characterization. ^{1}H NMR spectra were obtained using a JEOL JNM-ECA 300 spectrometer (300 MHz for proton). Relative molecular weights and molecular weight distributions were mea-

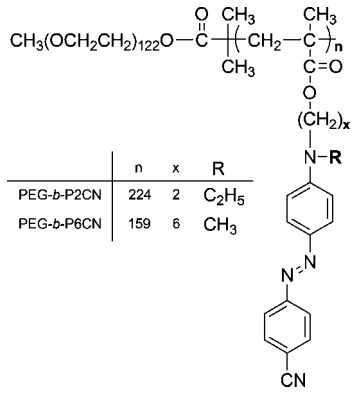

Figure 1. Chemical structures of PEG-*b*-P2CN and PEG-*b*-P6CN.

sured by the use of gel permeation chromatography (GPC) with THF as eluent at a flow rate of 1.0 mL/min. The instrument was equipped with a refractive index detector (Wyatt Optilab rEX) and fitted with a PLgel 5 μm mixed-D column. The measurement was carried out at 35 °C, and the results were calibrated with linear polystyrene standards. We tested thermal phase transitions of the polymers by using TA Instrument DSC 2920 with a heating rate of 10 °C/min under a nitrogen atmosphere. UV−vis spectroscopic measurements were performed on a Perkin-Elmer Lamba Bio-40 spectrophotometer. We obtained the atom force microscope (AFM) images by using a Nanoscope-IIIa scanning probe microscope in the tapping mode. Laser light scattering experiments were performed on a commercial LS instrument (ALV/DLS/SLS-5022F) equipped with a multi-τ digital time correlator (ALV/LSE-5003) and a solid-state laser (Uniphase, output power = 22 mW at λ = 632.8 nm). TEM observation was performed on a JEOL JSM-1200EX microscope with an accelerating voltage of 120 kV. We prepared samples for TEM observation by adding a droplet of the dispersions on a copper grid and allowing it to dry under the air-ambient condition.

Results and Discussion

Figure 1 shows the chemical structures of PEG-*b*-P2CN and PEG-*b*-P6CN. The copolymers consist of poly(ethylene glycol) (PEG) as the hydrophilic block and poly(2-(*N*-ethyl-*N*-(4-(4′-cyanophenyl-azo)phenyl)amino)ethyl methacrylate) (P2CN) or poly(6-(*N*-methyl-*N*-(4-(4′-cyanophenylazo)phenyl)-amino)hexyl methacrylate) (P6CN) as the hydrophobic block. Because of the inhibition of the pseudostilbene-type azo chromophores to free-radical polymerization, it is difficult to obtain the azo block copolymers directly through the ATRP method.[45] Therefore, the block copolymers were synthesized through a route that combines ATRP and postpolymerization azo-coupling reaction. The synthesis of PEG-*b*-P2CN was reported by us in a previous article.[44] PEG-*b*-P6CN was prepared by a similar method, which has been given in detail in the Experimental Section.

Block Copolymer Characterization. The GPC traces and ^{1}H NMR spectra of reaction intermediates and target copolymers are given in the Supporting Information (Figures S1−S3). The GPC results indicate the reasonable increases in the molecular weights through each reaction step, from macroinitiator (PEGBr) to the precursor polymers (PEG-*b*-PEMA and PEG-*b*-PHMA) and to the final azo diblock copolymers (PEG-*b*-P2CN and PEG-*b*-P6CN) after the azo-coupling reactions. The target azo block copolymers show narrow molecular weight distributions. ^{1}H NMR results reveal that nearly all anilino groups attached to the precursor polymers have been converted to azobenzene groups after the azo-coupling reactions. The resonance signal assignment and reaction conversion estimation can be seen in the Supporting Information as well as in our previous paper.[44] The high conversion of the postpolymerization azo-coupling reaction is consistent with previous reports.[15,44,45] The actual molecular weights of PEG-*b*-P2CN and PEG-*b*-P6CN were obtained from the ^{1}H NMR spectra by the following method. The repeat unit number of PEGBr was calculated to be 122, using the integral ratio of the resonance signals at 1.94 and 3.64 ppm. Then, we obtained the repeat unit numbers of the second block of PEG-*b*-PEMA and PEG-*b*-PHMA by comparing the integral areas of the signals corresponding to protons of the anilino groups and the PEG blocks. Because the azo-coupling reactions had a conversion of nearly 100%, PEG-*b*-P2CN and PEG-*b*-P6CN had the same block compositions as their precursor polymers. The molecular weight data obtained from both GPC and ^{1}H NMR are listed in Table 1. It can be seen that although the molecular weight of PEG-*b*-P6CN is smaller than that of PEG-*b*-P2CN, the weight ratios of the hydrophobic azobenzene-containing blocks to hydrophilic blocks are very similar for both polymers.

Table 1. Molecular Weight Data of the Macroinitiator, Precursor Copolymers, and Azo Diblock Copolymers, Which Were Obtained from GPC and ^{1}H NMR

sample	M_n (GPC)	M_n (^{1}H NMR)	PDI (GPC)	hydrophilic/hydrophobic blocks (wt/wt, ^{1}H NMR)
PEG	7600	5500	1.05	
PEG-*b*-PEMA	35 500	57 700	1.29	
PEG-*b*-PHMA	32 300	49 200	1.19	
PEG-*b*-P2CN	39 100	86 600	1.29	6/94
PEG-*b*-P6CN	34 000	69 700	1.23	7/93

The DSC heating curves (the second scan) of PEG-*b*-P2CN and PEG-*b*-P6CN are given in Figure 2. The result indicates that the two azo diblock copolymers show thermal properties of a typical amorphous polymer with T_g values of 117 °C for PEG-*b*-P2CN and 60 °C for PEG-*b*-P6CN. Although PEG is a semicrystalline polymer, no melting peak was detected during the DSC scan process. The observation could be attributed to the low weight fraction of PEG blocks in PEG-*b*-P2CN and PEG-*b*-P6CN, which did not form a crystalline domain through phase separation. The T_g values mainly correspond to the thermal behavior of the P2CN and P6CN blocks, which shows that T_g of the former is much higher. The UV−vis spectra of PEG-*b*-P2CN and PEG-*b*-P6CN, both in THF solutions and as spin-coated solid films, are given in Figure 3. The block copolymers show typical spectral characteristics of the pseudostilbene-type azobenzene chromophores. Only one strong absorption band appears in the visible wavelength range corresponding to the $\pi-\pi^*$ electron transition. The solid films of PEG-*b*-P2CN and PEG-*b*-P6CN show the maximum absorbance at 441 and 446 nm (λ_{max}). The λ_{max} of THF solutions of PEG-*b*-P2CN and PEG-*b*-P6CN appears at 443 and 449 nm, respectively. The slight red shifts of the THF solutions compared with the solid films can be attributed to the solvatochromic effect of the solvent.

Colloidal Sphere Formation and Characterization. The colloidal spheres of PEG-*b*-P2CN and PEG-*b*-P6CN were prepared by a method similar to that reported by Eisenberg et al.[46] We prepared homogeneous solutions by dissolving the copolymers in THF, which is a common solvent for both blocks

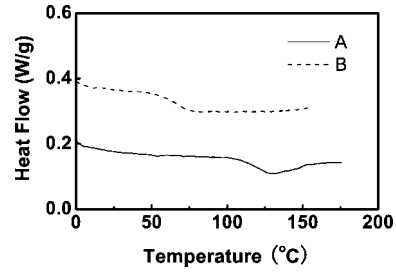

Figure 2. DSC curves of PEG-*b*-P2CN (curve A) and PEG-*b*-P6CN (curve B).

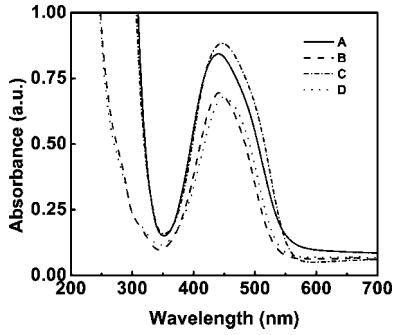

Figure 3. UV−vis spectra of PEG-*b*-P2CN spin-coated film (curve A), PEG-*b*-P2CN in THF solution (~0.01 g/L) (curve B), PEG-*b*-P6CN spin-coated film (curve C), and PEG-*b*-P6CN in THF solution (~0.01 g/L) (curve D).

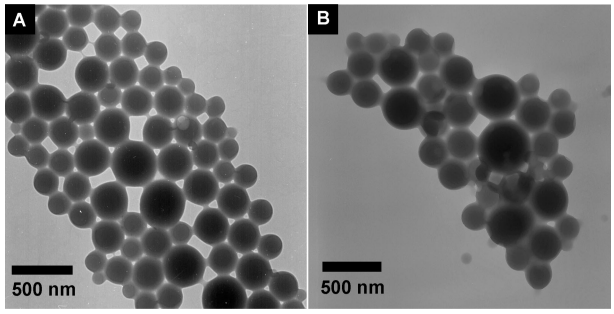

Figure 4. Typical TEM images of the colloidal spheres: (A) PEG-*b*-P2CN colloidal spheres prepared with the initial concentration of 0.2 g/L and the water-adding rate of 7.2 mL/h and (B) PEG-*b*-P6CN colloidal spheres prepared with the initial concentration of 0.2 g/L and the water-adding rate of 0.5 mL/h.

of the diblock copolymers. Then, deionized water was gradually added to the THF solutions to induce the hydrophobic aggregation, which was indicated by light scattering intensity variation (Figure S4 in the Supporting Information). After that, an excess amount of water was added to the dispersions to quench the formed structures, and THF was removed afterward to obtain the stable dispersions. To avoid possible influence of the colloidal size on the photoinduced deformation behavior, the sizes of the colloidal spheres were adjusted to be similar for both polymers. In general, the radii of colloidal spheres can be controlled by the initial concentration of polymer in organic solvent (C_{p0}) and the rate of water addition. The larger C_{p0} and slower water-adding rate result in the larger average radii of the colloidal spheres. In the present investigation, we prepared the colloidal spheres of PEG-*b*-P2CN and PEG-*b*-P6CN by using the same C_{p0} of 0.2 g/L. We prepared the colloidal spheres of both copolymers to possess analogous sizes by adjusting the water-adding rate.

Under these conditions, the block copolymers formed uniform colloidal spheres, as indicated by TEM observations (Figure 4). We statistically estimated the average radii $\langle R \rangle_n$ estimated from the TEM images by averaging the radii of 50 randomly selected particles. $\langle R \rangle_n$ of colloidal spheres of PEG-*b*-P6CN is 134 nm, which is slightly larger than that of PEG-*b*-P2CN (125 nm). The dynamic light scattering (DLS) results of the colloidal spheres are given in Figure 5. The z-average hydrodynamic radium ($\langle R_h \rangle_z$) of the PEG-*b*-P6CN colloids is 169 nm, which is slightly larger in comparison 144 nm for the PEG-*b*-P2CN colloidal spheres. The size distribution of the PEG-*b*-P6CN colloidal spheres is broader than that of the PEG-*b*-P2CN colloids, especially in the larger R_h side. The sizes of colloidal spheres, obtained from both TEM and DLS, are obviously larger than those estimated from the block lengths by assuming a typical micellar organization. The large sizes can be attributed

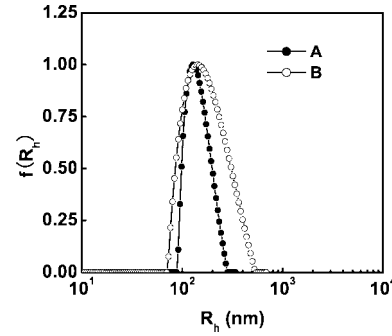

Figure 5. Hydrodynamic radius distribution of the colloidal spheres: PEG-*b*-P2CN colloidal spheres (curve A) prepared with the initial concentration of 0.2 g/L and the water-adding rate of 7.2 mL/h and PEG-*b*-P6CN colloidal spheres (curve B) prepared with the initial concentration of 0.2 g/L and the water-adding rate of 0.5 mL/h.

to the irreversible aggregation of the polymeric chains in the colloid formation process. It is believed that the "frozen" cores of the colloids were mainly composed of the hydrophobic azobenzene-containing blocks, but some PEG chains were also buried in cores. The shells of the colloids should be predominantly covered by the PEG blocks, which stabilized the aggregates in aqueous suspension.

Photoinduced Colloid Deformation Behavior. For the light irradiation test, the colloidal spheres were cast on TEM copper grids and dried properly under the ambient condition. The colloids were exposed to a linearly polarized Ar^+ laser beam (488 nm, 150 mW/cm^2) incident that was perpendicular to the grid surfaces. After different irradiation time periods, the samples were observed by TEM. The typical TEM images of the colloidal spheres after irradiation for different time periods are shown in Figure 6. It can be seen that the spherical aggregates are gradually elongated in the polarization direction of the laser beam as time increases. The average axial ratios (*l*/*d*) of the ellipsoidal particles, which were measured statistically from 50 particles, are used to describe the deformation degree. The relationship between the axial ratio and irradiation time is given in Figure 7. Both PEG-*b*-P2CN and PEG-*b*-P6CN colloidal spheres show a similar deformation pattern; that is, the axial ratios rapidly increase in the first 10 min, and then the increases begin to slow down until saturated values are achieved. However, a significant difference can be seen by comparing the two curves. Before saturation, the deformation rate of PEG-*b*-P2CN colloids is significantly faster than that of the PEG-*b*-P6CN colloids. Under the same irradiation conditions, the deformation degree of PEG-*b*-P2CN colloids is always larger than that of the PEG-*b*-P6CN colloids. It has been reported that the higher azo chromophore density can result in the larger deformation degree.[47] However, the azo chromophore density of PEG-*b*-P2CN colloids is only slightly higher than that of PEG-*b*-P6CN colloids, which could not cause such a large difference in the deformation behavior. The result reported here could be attributed only to the effect of the flexible spacers with different lengths.

Photoinduced Surface Relief Grating Formation Behavior. For comparison, SRG formation behavior of PEG-*b*-P2CN and PEG-*b*-P6CN was also studied. Homogeneous solid films of the copolymers with smooth surfaces were obtained by spin coating and vacuum drying at 40 °C for 24 h. Because the temperature was well below the T_g values of the copolymers, the possible phase separation was avoided, as confirmed by AFM phase images (Figure S5 in the Supporting Information). The SRGs were inscribed by the exposure of the films to the interference patterns generated by two linearly *p*-polarized Ar^+ beams. We monitored the SRG formation by measuring the first-

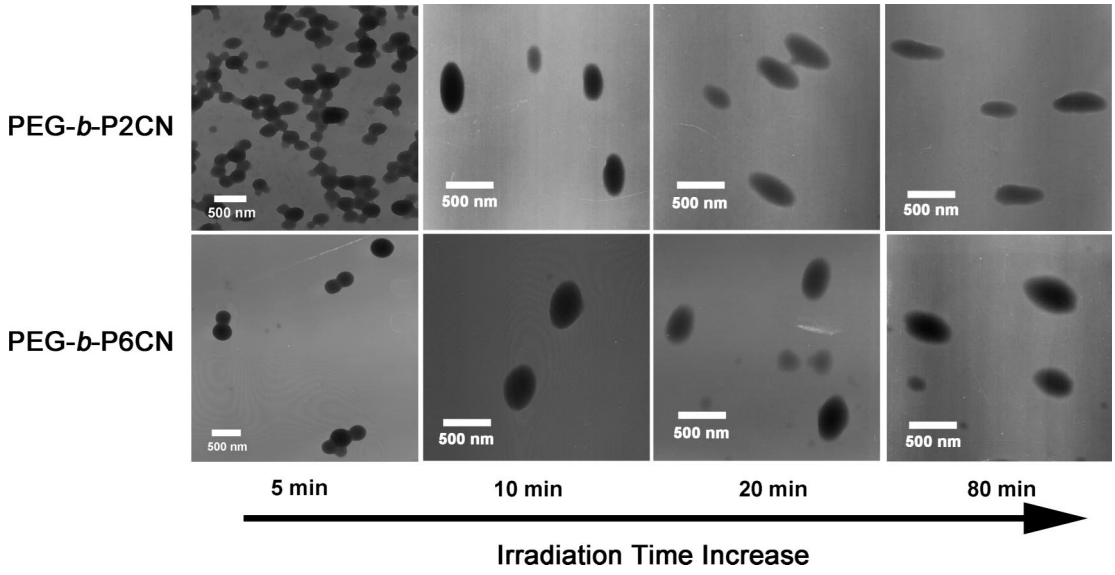

Figure 6. TEM graphs of PEG-*b*-P2CN and PEG-*b*-P6CN colloids in different irradiation stages.

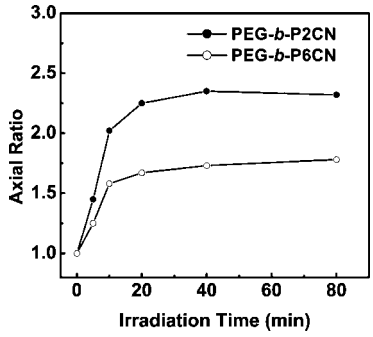

Figure 7. Plot of the average axial ratio (*l*/*d*) of the deformed PEG-*b*-P2CN and PEG-*b*-P6CN colloids versus the irradiation time.

order diffraction efficiency of a low-power He−Ne probe laser. The surface profiles of the gratings were characterized by AFM observation. The thicknesses of the copolymers films were controlled to be nearly the same, and the spatial periods of SRGs were adjusted to be in a range from 840 to 850 nm.

The 3D topography of SRGs inscribed on PEG-*b*-P2CN and PEG-*b*-P6CN films after light irradiation for the same time period (2600 s) is given in Figure 8. The modulation depths are 225 and 131 nm for the gratings on PEG-*b*-P2CN and PEG-*b*-P6CN films, respectively. Figure 9 shows the first-order diffraction efficiency as a function of irradiation time. The grating inscribed on PEG-*b*-P2CN film exhibits an obviously faster increase in the diffraction efficiency than that on PEG-*b*-P6CN film. The diffraction efficiency reaches 13.7% for PEG-*b*-P2CN and 5.3% for PEG-*b*-P6CN after irradiation for 2600 s. The lower diffraction efficiency for the gratings on PEG-*b*-P6CN film can be reasonably attributed to the smaller modulation depth. The data of diffraction efficiency and modulation depth both prove that SRGs can be more efficiently formed on the PEG-*b*-P2CN film compared with on the PEG-*b*-P6CN film.

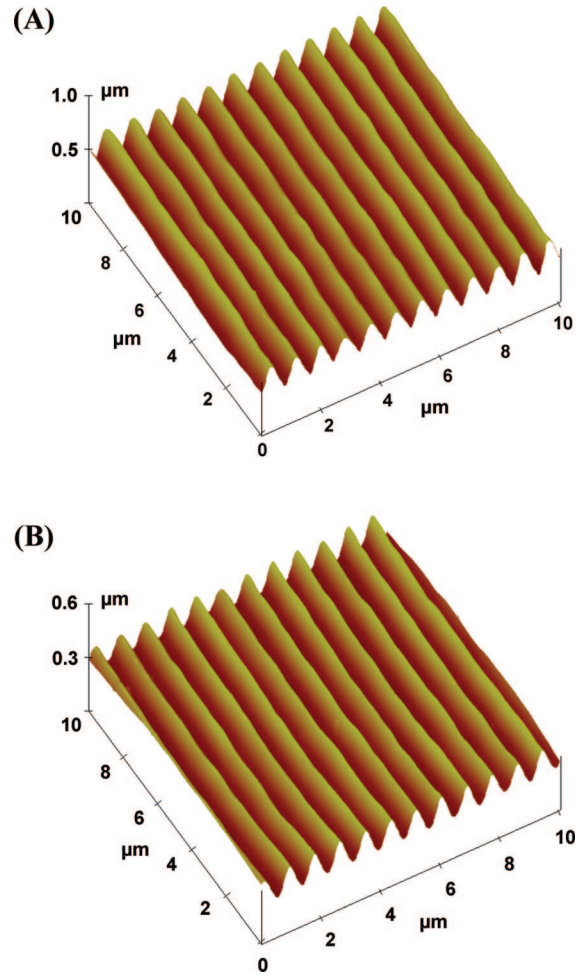

Figure 8. AFM 3D images of the surface profiles after Ar^+ laser irradiation for 2600 s: (A) PEG-*b*-P2CN film and (B) PEG-*b*-P6CN film.

Discussion

Both colloid deformation and SRG formation can be attributed to the photoinduced mass migration. The above results indicate that under similar conditions, light irradiation causes a more significant mass migration for PEG-*b*-P2CN colloids and thin films than it does for PEG-*b*-P6CN counterparts. The main structural difference between the two copolymers is that PEG-*b*-P6CN possesses longer flexible spacers between the polymeric main chain and the pendent azo chromophores. If the mass migration is driven by the azo chromophores, then the results could be reasonably explained by considering the function of the flexible spacers to transfer the driving force. The longer spacer might dissipate more driven energy obtained from the light irradiation. To understand the mechanism of the mass

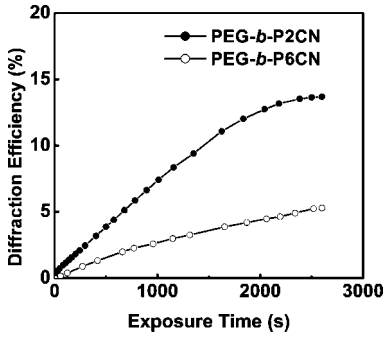

Figure 9. Diffraction efficiency of the surface relief gratings inscribed on PEG-*b*-P2CN and PEG-*b*-P6CN films as a function of irradiation time.

migration, the interaction between the azo chromophores and the irradiation needs to be considered in detail.

SRG formation has been attributed to the internal pressure gradient caused by an isomerization-driven free volume expansion in the bulk,[27] the force based on the dipolar interaction with the optically induced electric field gradient,[28] a translational wormlike diffusion caused by the photoisomerization of the azobenzene chromophores,[29] a mean-field force caused by the molecule alignment,[30] and photomechanical effect occurring in thin films of azo polymers.[31] The current observations could be partially elucidated by using the optical-field gradient force model proposed by Kumar et al.[28] For the SRG formation with interfering laser beam irradiation, the mass migration could be attributed to the optically induced electric field gradient related to the light intensity variation crossing the interference fringes. To consider the molecular details, the medium polarization used in the model as a key parameter should be replaced by the dipoles of the azo chromophores. In this case, the longer spacer would dissipate more driven energy of the light force exerting on the azo chromophores. For the colloid deformation induced by the irradiation with the linearly polarized laser single beam, the mass migration is more difficult to be explained by the same model and is believed to be related to the lens effect of spheres.[32b] In all of these cases, the repeated trans−cis−trans isomerization cycles of the azo chromophores should also play a key role. However, a detail molecular level explanation is still not available at the moment. To elaborate the current observations further, more systematic research is obviously needed, which includes the study of the photoinduced mass-migration behavior of other azo polymers with different spacer lengths and molecular structures.

Conclusions

We investigated the influence of the flexible spacer on the photoinduced mass-migration behavior by using two amphiphilic azobenzene-containing block copolymers (PEG-*b*-P2CN and PEG-*b*-P6CN) possessing ethylene and hexamethylene spacers. Uniform colloidal spheres of PEG-*b*-P2CN and PEG-*b*-P6CN were obtained by gradual hydrophobic aggregation induced by the increase in the water content in the THF−H_2O media. Upon irradiation with a linearly polarized Ar^+ laser beam, the colloidal spheres of PEG-*b*-P2CN showed a larger deformation rate and degree compared with the PEG-*b*-P6CN colloid spheres. Under irradiation of *p*-polarized interfering Ar^+ laser beams, SRG could be much more efficiently inscribed on PEG-*b*-P2CN films than on PEG-*b*-P6CN films. Both results indicate that the flexible spacers in the copolymers play a significant role in influencing the photoinduced mass-migration behavior.

Acknowledgment. Financial support from the NSFC under projects 50533040 and 20774055 is gratefully acknowledged.

Supporting Information Available: More characterization results of the block copolymer structures, aggregate formation, and film surface morphologies are given. This material is available free of charge via the Internet at http://pubs.acs.org.

References and Notes

(1) Kumar, G. S.; Nechers, D. C. *Chem. Rev.* **1989**, *89*, 1915–1925.
(2) Xie, S.; Natansohn, A.; Rochon, P. *Chem. Mater.* **1993**, *5*, 403–411.
(3) Delaire, J. A.; Nakatani, K. *Chem. Rev.* **2000**, *100*, 1817–1845.
(4) Natansohn, A.; Rochon, P. *Chem. Rev.* **2002**, *102*, 4139–4175.
(5) Ikeda, T.; Mamiya, J. I.; Yu, Y. L. *Angew. Chem., Int. Ed.* **2007**, *46*, 506–528.
(6) Ikeda, T.; Horiuchi, S.; Karanjit, D. B.; Kurihara, S.; Tazuke, S. *Macromolecules* **1990**, *23*, 42–48.
(7) Todorov, T.; Nikolova, L.; Tomova, N. *Appl. Opt.* **1984**, *23*, 4309–4312.
(8) Rochon, P.; Batalla, E.; Natansohn, A. *Appl. Phys. Lett.* **1995**, *66*, 136–138.
(9) Kim, D. Y.; Tripathy, S. K.; Li, L.; Kumar, J. *Appl. Phys. Lett.* **1995**, *66*, 1166–1168.
(10) Finkelmann, H.; Nishikawa, E.; Pereira, G. G.; Warmer, M. *Phys. Rev. Lett.* **2001**, *87*, 015501.
(11) Li, M. H.; Keller, P.; Li, B.; Wang, X. G.; Brunet, M. *Adv. Mater.* **2003**, *15*, 569–572.
(12) Yu, Y. L.; Nakano, M.; Ikeda, T. *Nature* **2003**, *425*, 145–145.
(13) Camacho-Lopez, M.; Finkelmann, H.; Palffy-Muhoray, P.; Shelley, M. *Nat. Mater.* **2004**, *3*, 307–310.
(14) (a) Natansohn, A.; Rochon, P.; Gosselin, J.; Xie, S. *Macromolecules* **1992**, *25*, 2268–2273. (b) Natansohn, A.; Xie, S.; Rochon, P. *Macromolecules* **1992**, *25*, 5531–5532. (c) Ho, M. S.; Barrett, C.; Paterson, J.; Esteghamatian, M.; Natansohn, A.; Rochon, P. *Macromolecules* **1996**, *29*, 4613–4618. (d) Barrett, C.; Choudhury, B.; Natansohn, A.; Rochon, P. *Macromolecules* **1998**, *31*, 4845–4851.
(15) (a) Wang, X. G.; Chen, J. I.; Marturunkakul, S.; Li, L.; Kumar, J.; Tripathy, S. K. *Chem. Mater.* **1997**, *9*, 45–50. (b) Wang, X. G.; Kumar, J.; Tripathy, S. K.; Li, L.; Chen, J. I.; Marturunkakul, S. *Macromolecules* **1997**, *30*, 219–225.
(16) (a) Hvilsted, S.; Andruzzi, F.; Ramanujam, P. S. *Opt. Lett.* **1992**, *17*, 1234–1236. (b) Hvilsted, S.; Andruzzi, F.; Kulinna, C.; Siesler, H. W.; Ramanujam, P. S. *Macromolecules* **1995**, *28*, 2172–2183.
(17) (a) Archut, A.; Vogtle, F.; De Cola, L.; Azzellini, G. C.; Balzani, V.; Ramanujam, P. S.; Berg, R. H. *Chem.—Eur. J.* **1998**, *4*, 699–706. (b) Archut, A.; Azzellini, G. C.; Balzani, V.; De Cola, L.; Vogtle, F. *J. Am. Chem. Soc.* **1998**, *120*, 12187–12191. (c) Schenning, A. P. H. J.; Elissen-Roman, C.; Weener, J. W.; Baars, M. W. P. L.; van der Gaast, S. J.; Meijer, E. W. *J. Am. Chem. Soc.* **1998**, *120*, 8199–8208.
(18) (a) Junge, D. M.; McGrath, D. V. *Chem. Commun.* **1997**, 857–858. (b) Junge, D. M.; McGrath, D. V. *J. Am. Chem. Soc.* **1999**, *121*, 4912–4913.
(19) (a) Nagasaki, T.; Tamagaki, S.; Ogino, K. *Chem. Lett.* **1997**, 717–718. (b) Yokoyama, S.; Nakahama, T.; Otomo, A.; Mashiko, S. *Chem. Lett.* **1997**, 1137–1138. (c) Yokoyama, S.; Nakahama, T.; Otomo, A.; Mashiko, S. *J. Am. Chem. Soc.* **2000**, *122*, 3174–3181.
(20) (a) Wang, G. J.; Cheng, H.; Wang, X. G. *Chem. Lett.* **2002**, 78–79. (b) He, Y. N.; Wang, X. G.; Zhou, Q. X. *Synth. Met.* **2003**, *132*, 245–248. (c) Che, P. C.; He, Y. N.; Wang, X. G. *Macromolecules* **2005**, *38*, 8657–8663.
(21) Tian, Y. Q.; Watanabe, K.; Kong, X. X.; Abe, J.; Iyoda, T. *Macromolecules* **2002**, *35*, 3739–3747.
(22) Wang, G.; Tong, X.; Zhao, Y. *Macromolecules* **2004**, *37*, 8911–8917.
(23) Han, Y. K.; Dufour, B.; Wu, W.; Kowalewski, T.; Matyjaszewski, K. *Macromolecules* **2004**, *37*, 9355–9365.
(24) Sin, S. L.; Gan, L. H.; Hu, X.; Tam, K. C.; Gan, Y. Y. *Macromolecules* **2005**, *38*, 3943–3948.
(25) (a) Yu, H. F.; Okano, K.; Shishido, A.; Ikeda, T.; Kamata, K.; Komura, M.; Iyoda, T. *Adv. Mater.* **2005**, *17*, 2184–2188. (b) Yu, H. F.; Iyoda, T.; Ikeda, T. *J. Am. Chem. Soc.* **2006**, *128*, 11010–11011.
(26) Morikawa, Y.; Nagano, S.; Watanabe, K.; Kamata, K.; Iyoda, T.; Seki, T. *Adv. Mater.* **2006**, *18*, 883–886.
(27) (a) Barrett, C. J.; Natansohn, A. L.; Rochon, P. L. *J. Phys. Chem.* **1996**, *100*, 8836–8842. (b) Barratt, C. J.; Rochon, P. L.; Natansohn, A. L. *J. Chem. Phys.* **1998**, *109*, 1505–1516.
(28) (a) Kumar, J.; Li, L.; Jiang, X. L.; Kim, D. Y.; Lee, T. S.; Tripathy, S. *Appl. Phys. Lett.* **1998**, *72*, 2096–2098. (b) Bian, S. P.; Williams, J. M.; Kim, D. Y.; Li, L.; Balasubramanian, S.; Kumar, J.; Tripathy, S. *J. Appl. Phys.* **1999**, *86*, 4498–4508.
(29) Lefin, P.; Fiorini, C.; Nunzi, J. M. *Pure Appl. Opt.* **1998**, *7*, 71–82.
(30) Pedersen, T. G.; Johansen, P. M.; Holme, N. C. R.; Ramanujam, P. S.; Hilvsted, S. *Phys. Rev. Lett.* **1998**, *80*, 89–92.
(31) (a) Tanchak, O. M.; Barrett, C. J. *Macromolecules* **2005**, *38*, 10566–10570. (b) Yager, K. G.; Tanchak, O. M.; Godbout, C.; Fritzsche, H.;

Barrett, C. J. *Macromolecules* **2006**, *39*, 9311–9319. (c) Yager, K. G.; Barrett, C. J. *Macromolecules* **2006**, *39*, 9320–9326.
(32) (a) Li, Y. B.; He, Y. N.; Tong, X. L.; Wang, X. G. *J. Am. Chem. Soc.* **2005**, *127*, 2402–2403. (b) Li, Y. B.; He, Y. N.; Tong, X. L.; Wang, X. G. *Langmuir* **2006**, *22*, 2288–2291.
(33) Lambeth, R. H.; Moore, J. S. *Macromolecules* **2007**, *40*, 1838–1842.
(34) Finkelmann, H.; Ringsdorf, H.; Wendorff, H. J. *Makromol. Chem.* **1978**, *179*, 273–276.
(35) Gemmell, P. A.; Gray, G. W.; Lacey, D.; Alimoglu, A. K.; Ledwith, A. *Polymer* **1985**, *26*, 615–621.
(36) Winkler, B.; Ungerank, M.; Stelzer, F. *Macromol. Chem. Phys.* **1996**, *197*, 2343–2357.
(37) Yamaki, S.; Nakagawa, M.; Morino, S.; Ichimura, K. *Macromol. Chem. Phys.* **2001**, *202*, 354–361.
(38) Wu, Y. L.; Demachi, Y.; Tsutsumi, O.; Kanazawa, A.; Shiono, T.; Ikeda, T. *Macromolecules* **1998**, *31*, 1104–1108.
(39) Cha, S. W.; Choi, D. H.; Oh, D. K.; Han, D. Y.; Lee, C. E.; Jin, J. I. *Adv. Funct. Mater.* **2002**, *12*, 670–678.
(40) Han, M.; Ichimura, K. *Macromolecules* **2001**, *34*, 82–89.
(41) Freiberg, S.; Lagugne-Labarthet, F.; Rochon, P.; Natansohn, A. *Macromolecules* **2003**, *36*, 2680–2688.
(42) Labarthet, F. L.; Freiberg, S.; Pellerin, C.; Pezolet, M.; Natansohn, A.; Rochon, P. *Macromolecules* **2000**, *33*, 6815–6823.
(43) Han, M.; Kidowaki, M.; Ichimura, K.; Ramanujam, P. S.; Hvilsted, S. *Macromolecules* **2001**, *34*, 4256–4262.
(44) Wang, D. R.; Ren, H. F.; Wang, X. Q.; Wang, X. G. *Macromolecules* **2008**, *41*, 9382–9388.
(45) (a) Wang, D. R.; Ye, G.; Wang, X. G. *Macromol. Rapid Commun.* **2007**, *28*, 2237–2243. (b) Wang, D. R.; Liu, J. P.; Ye, G.; Wang, X. G. *Polymer* **2009**, *50*, 418–427.
(46) Zhang, L. F.; Eisenberg, A. *J. Am. Chem. Soc.* **1996**, *118*, 3168–3181.
(47) Liu, J. P.; He, Y. N.; Wang, X. G. *Langmuir* **2008**, *24*, 678–682.

MA8026063